# Catalysis Science & Technology

Accepted Manuscript






ROYAL SOCIETY OF CHEMISTRY

www.rsc.org/catalysis

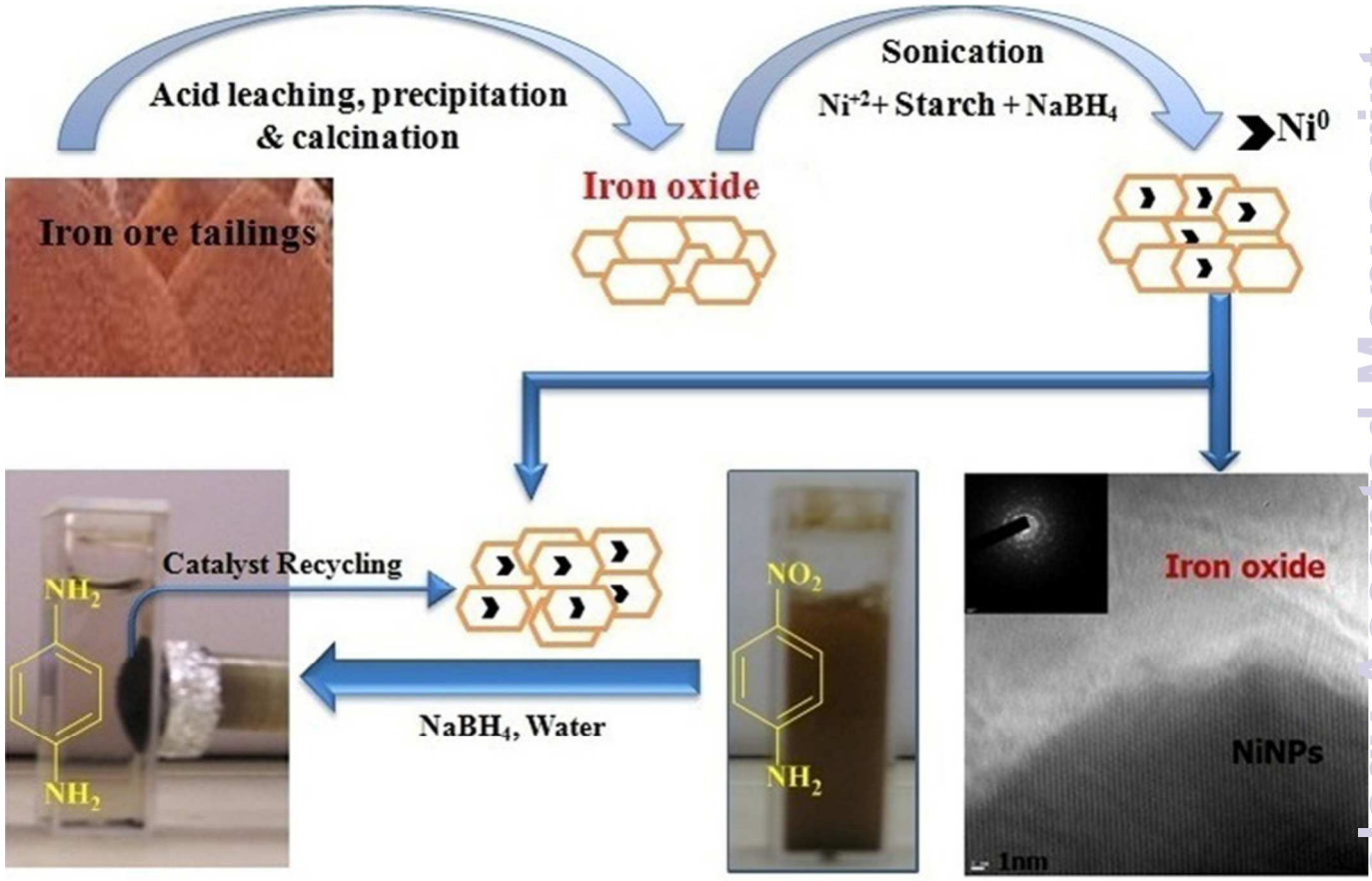

# Magnetically separable core/shell Iron oxide@Nickel nanoparticles as high-performance recyclable catalysts for chemoselective reduction of nitroaromatics

Puran Singh Rathore[a], Rajesh Patidar[b], T. Shripathi[c], Sonal Thakore[a]*

[a]Department of Chemistry, Faculty of Science, The M. S. University of Baroda, Vadodara, 390002, India

[b]Analytical Discipline and CIF, Central Salt and Marine Chemicals Research Institute (CSIR-CSMCRI), G. B. Marg, Bhavnagar, 364002, Gujarat, India

[c]UGC-DAE Consortium for Scientific Research, Indore 452 001, India

## Abstract

A magnetically separable core-shell Iron oxide @Nickel (IO@Ni) nanocatalyst was synthesized by reduction of $Ni^{+2}$ ions in the presence of iron oxide ($Fe^{+2}$, $Fe^{+3}$) by a simple one-pot synthetic route using $NaBH_4$ as reducing agent and starch as capping agent. The synthesized nanoparticles (NPs) were characterized by several techniques such as X-ray diffraction pattern (XRD), high resolution transmission electron microscopy (HR-TEM), selected area electron diffraction (SAED) pattern, and energy dispersive X-ray spectroscopy (EDS). The core-shell Iron oxide@Nickel nanoparticles (IO@NiNPs) was found to have very excellent activity for the hydrogenation reactions of aromatic nitro compounds under mild conditions using water as green solvent. Excellent chemoselectivity and recyclability up to 30 cycles for the nitro group reduction was demonstrated.

**Keywords:** Iron oxide, Magnetic separation, Nickel nanoparticles, catalysis, core/shell, Reduction.

*Author for correspondence: Phone no. 91-0265-2795552, Fax: 91-0265-2429814

*E – mail ID: chemistry2797@yahoo.com*

## Introduction

The concept of ‘‘Green Chemistry’’ has come out as one of the guiding principles of environmentally benign synthesis.[1–3] Nanomaterials-catalyzed transformations in an aqueous reaction medium are one of the ideal solutions for the development of green and sustainable protocols. Nanocatalysis is a rapidly growing field which involves the use of metal nanoparticles as catalysts for a variety of organic reactions.[4] The preparation and use of magnetic nanoparticles (MNPs) offers advantages in clean and sustainable chemistry as they are non-toxic, readily accessible, and retrievable.[5] Additionally, the activity and selectivity of magnetic nano-catalysts can be manipulated by their surface modification.

The development and design of core-shell nanomaterials has emerged in recent years because of their multifaceted applications especially as catalysts for organic reactions.[6,7] Magnetically separable nanocatalyst is an important class of the core-shell nanocatalyst family which are robust, air stable, avoid traditional filtration processes and are recyclable.[8] Various methods have been developed to synthesize specific application based MNPs.[9–13] Some of them are aimed at developing materials from waste such as iron tailings. Tailings refer to waste material of beneficiation processes. Among several iron based solid waste, iron ore tailings (IOTs) is one of the fast accumulating wastes throughout the world due to rapid expansion of iron and steel based industries and is becoming one of the serious environmental threats for the future generation. Presently IOTs are mainly used with very little intervention of high technology and moreover value addition is low. As a result there is an increasing interest in search of possible alternative uses of waste IOTs such as adsorption and catalysis or as precursors to value added

products before their final discharge.[14-19] Here we assess the potential of synthesizing magnetic iron oxide from IOTs and use as template for synthesis of magnetically separable nickel nanoparticle (NiNPs).

The reduction of nitroarenes is an important process as the products, aromatic amines, are versatile intermediates and precursors in the preparation of dyes, pharmaceuticals, pigments, agrochemicals and polymers.[20] The process is complicated as the reduction of a nitro group proceeds in stages and it often stops at an intermediate stage producing hydroxylamine and hydrazine as side products.[21] A variety of procedures and reducing agents are available for this purpose.[22] In literature a few procedures involving noble metal NPs such as Pd, Pt, Ag, Au, as well as Fe, $Fe_3O_4$@Ni and Ni@Ag NPs have been demonstrated for the reduction of nitro group.[22-24,7] The main limitations of earlier reported work were the necessity of high $H_2$ pressures, prolong reaction time, lower turnover number, organic solvents, less recyclability and high temperatures. Further, the selection of metal and its support, the hydrogen source and operational simplicity, which are the important parameters for effective conversions, are restricted. However, an alternative efficient, simple, chemoselective, green and cost-effective procedure is highly appreciated.

In the past, we have investigated the use of NiNPs as catalysts for transesterification as well as reduction.[25] In this paper, we report the first protocol for the synthesis of starch capped iron oxide@Ni (IO@Ni) core-shell magnetically separable nanocatalyst for hydrogenation of aromatic nitro compounds. Initially *p*-Nitroaniline (PNA) was used as the model system to simplify the analysis and to accelerate the screening speed. All reactions were carried out at room temperature (rt) in aqueous medium (Green solvent).

Consequently the optimized conditions were used for the synthesis of various aromatic amines.

## Results and Discussions

### Synthesis and characterizations of Iron oxide (IO)

The IOTs, selected for the present study, primarily constitute of Fe, Si and Al with magnetite, hematite and goethite as the main iron bearing phases (Supporting information). Si and Al are present in the form of kaolinite which is evident from X-ray diffraction (XRD) patterns (Supporting information). Fig. 1A shows XRD of as synthesized IO. The lines in the Fig. 1A correspond to crystalline phases. It is from the pattern that sample is composed of mixed phases. The detail analysis has been carried out based on Crystallography Open Database (COD). All the crystallite lines identified with respective phase(s) are shown in the Fig. 1. Details of compositions along with its peak positions are shown in supporting information. It is also observed that pattern is dominated by maghemite ($\gamma$-$Fe_2O_3$) and magnetite ($Fe_3O_4$) phases. It is to be noted here that the peak positions of both the phases are very nearby to each other, hence exact identification is very difficult. However, based on the intensity distribution, it can be concluded that the sample consists of majority of maghemite or magnetite phase along with hematite as secondary phase and goethite as impurity phase. XRD pattern is similar to reported data.[26-27] SEM-EDX of IO also showed the presence of Fe metal (Supporting information).

### Synthesis and characterizations of IO@NiNPs

Template synthesis method was used for synthesis of magnetic separable core/shell nanoparticles. This method is mainly used to generate specific nanostructures of

bimetallic nanoalloys which are otherwise very difficult to prepare. This approach utilizes pre-formed iron oxide of the first metal and subsequently directing the deposition of the Ni metal onto a surface site. In the present study nanosized nickel was deposited on iron oxide under sonication and using starch as capping agent. This method is commonly used to prepare core–shell or multi-shell morphologies. Starch capping was proved by FT-IR (Supporting information).

Fig.1B shows the XRD pattern of IO@NiNPs. The signals of Ni were not detected in the XRD spectrum of IO@NiNPs although the position and relative intensity of diffraction peaks are reasonably close to the reported pattern.[24b,28] XRD pattern shows that the MNPs are well-crystalline and exhibit diffraction peaks corresponding to (111), (220), (311), (400), (511) and (440) planes of cubic crystal system. XRD pattern indicate mixed phases of iron oxides with Nickel.

The weight percentage of Ni was determined to be 1.98 % by AAS analysis and Energy Dispersive X-ray Analysis (EDX) also confirm the ratio 1.89:98.11 (Ni/Iron oxide) (Fig. 2A). EDX analysis indicates that the well-cleaned final product is mostly composed of O, Fe and Ni, with no other signal (Fig. 2A).

The magnetic measurements have been carried out at room temperature, and the data are shown in Figure 2B, on the as-prepared iron oxide and IO@NiNPs. From the recorded M−H loop, it is clear that both the as-prepared samples are ferromagnetic at RT. The magnetization of the as-prepared iron oxide was 1.6269 emu, and it decreased to a value of 1.5259 emu after coating of NiNPs. The coercivity values of the IO and IO@NiNPs were 73.65 and 61.76 G, respectively. The low magnetization value exhibited by the IO@NiNPs compared to the iron oxide one could be due to the presence of

impurities/defects in the IO@NiNPs. Since the size of nanoparticles synthesized by us lies in the range of 20−50 nm, they are still ferromagnetic.

In order to give further evidence of formation of NiNPs shell over the iron oxide core and to determine the oxidation state of Ni, XPS resolution Ni 2p spectroscopy results of iron oxide and IO@NiNPs were compared (Supporting information). The signals of Ni were very faint in the XPS spectrum of IO@NiNPs (Fig. 3) because of low loading of Nickel metal. Nevertheless, for a better understanding of the oxidation state of Ni metal, the binding energy obtained from the catalyst was compared with the Ni metal $2p_{3/2}$ peak position. The peak value obtained at 852.9 eV is within the range of literature value (852.7 eV ± 0.4 eV).[29] In agreement with the above analyses, it can be concluded that oxidation state of nickel in the catalyst is zero.

The Brunauer-Emmet-Teller (BET) surface area of a magnetic IO@NiNPs sample was determined to be 17.6546 $m^2/g$, these MNPs have high surface area (supporting information). The pore size of the MNPs was determined to be 25.4629 nm by the Barrett-Joyner-Halenda (BJH) analysis of the isotherms (supporting information). The total pore volumes were 0.051547$cm^3/g$ (supporting information). The High-Resolution Transmission Electron Microscopy (HR-TEM) images of IO@NiNPs are shows somewhat spherical morphology with some cubic partials an average size range of 20–50 nm (Fig. 4A). Fig. 4B and C are HR-TEM images of typical IO@NiNPs at different magnifications. The high resolution images in Fig. 4D and E shows well developed lattice fringes and the fringes extend throughout the particle confirming the monocrystalline nature of the individual particles. The distance between adjacent lattice fringes measured as 0.221nm in Fig. 4D corresponds to the 311 reflection. The selected

area electron diffraction (SAED) pattern shown in Fig. 4F corresponds to the higher order reflections of IO@NiNPs.[30] The HR-TEM image (Fig. 4) clearly shows that nickel is deposited on the iron oxide surface. In accordance with the above analyses, it can be concluded that the nanoparticles prepared in this method are mixture iron oxide with nickel metal nanoparticles.

**Catalytic reduction of *p*-Nitroaniline and other aromatic nitro compounds**

The IO@Ni core-shell nanoparticles were used as catalyst for the hydrogenation of aromatic nitro compounds using $NaBH_4$ as the hydrogen donor and water as solvent as shown in Scheme-1. For Initial screening reduction of *p*-Nitoaniline (PNA) to yield *p*-Phenylenediamine (PPDA) was investigated under various reaction conditions (table-1). The conversion was monitored by UV-vis spectrophotometer, where the product and reactant show different absorption bands at 307nm and 381nm, respectively as shows in Fig. 5.

It is seen from the Table-1 (entries 1-3) that the presence of a catalyst along with $NaBH_4$ is required for hydrogenation of PNA. In our previous study we have observed that nickel nanoparticle catalysed hydrogenation of PNA takes more than one hour.[25b] When the reaction was carried out using only IO, the reaction yields was very low (~ 50 to 55%) even after 24h at rt (Table-1, entry-4). When the reaction conditions mentioned in the Table (entry-6) were used, the reaction proceeded faster within 12 min and the $\lambda_{max}$ shifted from 381nm to 307nm. Whereas, in the absence of NPs, the peak at 381nm corresponding to PNA did not disappear even after 24h of reflux. The optimum reaction conditions for PNA reaction are given in table-1 (entry 6), which yields 96±2 % of product at rt after 12min and selectivity was 100%.

Nanocatalysts can catalyze the reduction of nitro compounds by acting as an electronic relay system to overcome the kinetic barrier, in which the electrons donated by $BH_4^-$ can be transferred to the acceptor nitro groups.[31] The *p*-Nitroaniline and $BH_4^-$ were adsorbed by the electronic hole in the surface of the NiNPs via chemical adsorption. Immediately, *p*-Phenylenediamine was produced on the surface of NPs. In the second step, the PPDA was desorbed from the surface of the NPs. A detailed mechanism has been proposed by Xie *et al*.[32]

Furthermore, experiments were performed using a different mole ratio of $NaBH_4$ in standard reaction. When we decrease moles of $NaBH_4$ from 1.85 mmol to 1.44 mmol the yield and reaction time did not change (table-1, entry 5 and 6), whereas using 1.44 mmol of $NaBH_4$ resulted into a remarkable yield (96±2%) at 25-30°C within 12min (table-1, entry 6). However, further lowering the amount of $NaBH_4$ caused an increase in the reaction time (entry 6 to 10) and hence an adequate quantity of $NaBH_4$ was used in optimum reaction condition.

Variation in quantity of NPs (table-1, entries 11 to 16) under optimum reaction conditions showed that even 0.3 mg was sufficient for catalyzing the reaction at rt. But the reaction time increased to 180 min for maximum conversion (table-1, entry 16). On the other hand with 9 mg the reaction time decreased to 23min (table-1, entry 9). Beyond 12 mg the reaction time and yield did not change (table-1, entries 11 and 12).

In order to assess the efficiency of the NPs further, the quantity of water and substrate were also optimized (Supporting information). After optimization of the reaction conditions (table-1and Supporting information) the catalytic activity of magnetic IO@Ni core-shell NPs, with other nitro substrates was further explored (Scheme-2). The catalytic

performance of the nanocatalyst, was not significantly influenced by the nature and position of the substituents on the aromatic nitro compounds. Electron-donating as well as -withdrawing groups such as –Cl, –Br, $CH_3$ and –OH did not have significant influence on the reaction (Table 2). Notably, electron transfer over IO@Ni core-shell nanocatalyst exhibits excellent activity and selectivity for the hydrogenation of a series of halogenated nitrobenzenes to the corresponding halogenated amines, without any dehalogenation (Table 2, entries 10, 11, 16-20 and 23). All the nitro arenes were reduced in excellent yields affording a single product, which minimizes the efforts to separate unreacted starting compounds. In all cases, the turnover number (TON) was as high as ~102 to 115 and turnover frequency (TOF) ~ 2 to 12 per site per min. (Table-2).

Further, this catalytic system works efficiently in aqueous system and therefore no hazardous solvent was required. This reaction has been investigated in the presence of other protic solvents such as methanol, ethanol, and ethylene glycol; however, none of them gave satisfactory results (data not given). In an aqueous system $NaBH_4$ gives sodium metaborate ($NaBO_2$)[33] which is the only waste generated during the reaction. However sodium metaborate can be recycled using magnesium hydride ($MgH_2$) or magnesium silicide ($Mg_2Si$) by annealing (350–750◦C) under high $H_2$ pressure (0.1–7 MPa) for 2–4 h.[33] This opens up new possibilities for eco-friendly synthesis of aromatic amines.

**Recycling of IO@NiNPs**

The IO@Ni core-shell NPs were recovered by external magnetic separation (Figure-5A; a and b) with negligible loss. Recycling experiments carried out under optimized conditions showed interesting results. It was observed that the NPs could be reused

directly without further purification for 30 consecutive runs as can be seen in Table-3 with very high total turnover number (TTN) 3456. Up to 16 cycles there was no loss in activity. After that, however, the reaction time increased with each successive recycling experiment reaching from 12 min to 140 min finally. This may be due to gradual loss of the catalytic activity of the nanocatalyst with number of runs which may be due to various reasons. One of the reasons may be surface modification due to deposition of matter during reaction.[34] The HR-TEM images of the nanocatalyst recorded after 30$^{th}$ run displays an agglomeration of NPs due to deposited matter (Fig.6B and C). The image in Fig. 6D shows that lattice fringes were damaged by deposited matter throughout the particle. The SAED pattern shown in Fig. 6E corresponds to the reflections of IO@NiNPs still confirming the crystalline nature of the catalyst; but the catalytic activity reduces due to deposited matter. Nevertheless, the reaction does proceed to completion at the same temperature at the end of 30 cycles giving the same yield. Further the reused IO@NiNPs was also characterized by EDX and atomic absorption spectrophotometer (AAS) to confirm the leaching of nickel during reaction. EDX analysis reveals that the Ni content in IO@NiNPs which was 1.89% before the reaction showed a marginal decrease to 1.53% (Fig. 6F) after the reusability study of 30 cycles. This confirmed that only negligible leaching of nickel occurred which was further supported by AAS results (Supporting information). Ferrous and ferric ion leaching were also ensured by AAS (Supporting information). High recyclability and stability of IO@NiNPs can be attributed to the presence of starch coating which makes the IO@NiNPs stable to water and air and maintains the metallic state of nickel in catalyst.[35] This eventually increases their utility

and enhances recycling efficiency. Thus the metal surface, capping agent and $NaBH_4$ simultaneously make the IO@NiNPs system an effective catalyst.

## Conclusion

The present study demonstrated the feasibility of using a waste from iron ore beneficiation plants (IOTs) as one of the starting materials for the synthesis of IO@Ni core-shell MNPs and its possible applications in the catalysis. A highly efficient, viable heterogeneous IO@Ni core-shell MNPs catalyst was developed for hydrogenation reaction using environment friendly solvent water. Due to sturdy interaction between NiNPs and iron oxide, the catalyst could be reused by recycling 30 times, without any significant loss in catalytic activity and selectivity. The reaction was broadly applicable as diverse aromatic nitro compounds were successively converted to the corresponding amines in excellent yield (85–96%), high TON and TOF. Being robust and magnetically separable, this core-shell catalyst is a promising candidate for other important organic conversions and industrial applications. Further investigation, modification, and applications are under progress in our laboratory.

## Experimental

### Materials

*p*-Nitroaniline (PNA), other aromatic nitro compounds, $NaBH_4$, $Ni(CH_3COO)_2.4H_2O$, liquid ammonia, and starch were purchased from Merck Mumbai, India. All the solutions were prepared using double-distilled and demineralized water. Iron ore tailings, collected from iron industries (Silverline Exporters Private Limited, Gujarat, India), and were screened for their iron contents and one sample with relatively high iron content (~36.04%) was used as one of the starting materials.

**Synthesis of Iron oxide**

Mixture of iron oxide was synthesized from the waste iron ore tailings (IOTs) via acid leaching and precipitation through a sequential precipitation method, as previously reported.[35] For almost complete recovery of iron from IOTs it was first neutralization by adding $Ca(OH)_2$ followed by the settling of aluminium hydroxide and calcium sulfate; subsequently neutralization by adding NaOH and precipitation of $Fe(OH)_2$. The $Fe(OH)_2$ was gradually oxidized to iron oxide. The thermal treatment of iron oxide was performed in an oven, after drying at 100 °C, at 450 °C temperature. Further details on the synthesis of iron oxide is discussed elsewhere.[36-38] These results indicate that IOTs could be used as a source material for the production of iron oxide, with comparable quality to those produced using analytical-grade reagents.

**Synthesis of Iron oxide@Nickel Nanoparticles (IO@NiNPs)**

IO@Ni core@shell NPs were synthesized by reduction of $Ni^+$ ions in the presence of iron oxide. To deposit NiNPs, 100 mg of iron oxide was dispersed in 10mL of deionized water and sonicated for 30 min. Nickel Nanoparticles were synthesized on magnetic core through a wet chemical reduction process by earlier reported method with minor modifications.[25b] $Ni(CH_3COO)_2.4H_2O$ and soluble starch were used as metal salt precursor and stabilizing agent respectively. $NaBH_4$ (10%, W/V) was used as reducing agent and liquid ammonia as complexing agent. Briefly 10 ml of 0.02M nickel acetate solution was added to 10 ml of starch solution (1%, W/V) and stirred on a magnetic stirrer at RT. The pH of the solution was adjusted to 10 with liquid ammonia (600µL) and reduction was carried out with 200 µL of $NaBH_4$ solution. On further stirring for 10 min. the IO were gradually coated by NiNPs when the colour of the solution changed from red

to reddish black. The resultant IO@NiNPs were collected by external magnet and washed by deionized water several times to remove unreacted materials. Finally NPs were washed with acetone, and dried at 60 °C under a vacuum.

**Catalytic reduction of *p*-Nitroaniline and other aromatic nitro compounds**

In a typical reaction PNA 50mg (0.362 mmol) was used as a starting material, $NaBH_4$ 54.6mg (1.44 mmol) as a source of hydrogen, water (2 mL) as a solvent and IO@Ni-MNPs 12mg (0.45 wt% NiNPs of PNA) as a nanocatalyst. All the components were mixed together in 10 mL round bottom flask and the reaction was carried out at room temperature (rt, 25-30 °C) under stirring for 12 min. Reaction monitoring was done by thin-layer chromatography (TLC) and gas chromatography. After completion of the reaction, catalyst was separated magnetically. The product was isolated by extraction in dichloromethane and evaporation of solvent followed by column chromatography (10:90, ethyl acetate in hexane v/v) over basic alumina furnished *p*-Phenylenediamine (PPDA). The spectroscopic data of this compound are in good agreement with those reported. The reaction was also carried out with IO, NiNPs and without catalyst for comparison.

Reduction of other nitro aromatics was carried out in a similar manner. The products purified by short-path basic alumina chromatography (0-40% ethyl acetate in hexane v/v) were analyzed by $^1$HNMR (Supporting information).

All experiments have been repeated three times and the reproducibility confirmed. The recyclability of the NPs was also surveyed. The NPs were recovered by magnet and washed with water followed by methanol and again water. They were dried at 60 ºC under vacuum and used for the next cycle.

**Characterizations methods**

The chemical analyses for major constituents in IOT, acid insoluble residue and aqueous suspension of IO@NiNPs were carried out by conventional wet chemical analysis while AAS (AA 6300: Shimadzu, Japan) or ICP-OES (Perkin Elmer, 4300) was used to analyze the constituents present in traces. The powered X-ray diffraction (XRD) patterns were recorded with a PanAlytical (model; Empyrean) 'X'PERT-PRO XRPD of Cu Kα radiation (λ= 0.15406 nm) on advance X-ray power diffractometer. Samples were prepared by pressing dried powder and patterns were collected with scanning rate of 2°/min and 2θ ranging from 0 to 80°. Surface area and porosity of the nanocatalyst were measured by a volumetric adsorption system (Micromeritics Instrument corporation, USA, model ASAP 2010) using $N_2$ adsorption/desorption isotherms at 77 K upto 1 bar. Prior to the measurements, the samples were activated (degassed) by heating at the rate of 1 K/min upto 383 K under vaccum. The temperature as well as vacuum was maintained for 7 hours prior to the measurements. Surface area was calculated by Brunauer-Emmet-Teller (BET) method while the porosity by Barrett-Joyner-Halenda (BJH) method. High-Resolution Transmission Electron Microscopy (HR-TEM) was carried out using Jeol (Jem-2100) electron microscope operated at an acceleration voltage of 200 kV. For this purpose, dry powered sample was dispersed in methanol and ultrasonication treatment was given for 30 min. After that sample was deposited onto a carbon-coated grid at room temperature and it was allowed for air-drying (about 6 hours). Selected area electron diffraction patterns (SAED) and Energy-dispersive X-ray spectroscopy (EDX/EDS) were also investigated from the electron micrographs. FT-IR spectra were recorded as KBr pellet on Perkin Elmer RX1 model in the range of 4000-400 $cm^{-1}$. Magnetic measurements were done by a vibrating sample magnetometer (EG&G Model 155 VSM)

at room temperature in the range +20,000 to −20,000 G. The surface composition was investigated using X-ray Photoelectron Spectroscopy (XPS) on VSW X-ray photoelectron spectrometer (UK) using Mg and Al twin anode X-ray gun with multichannel detector and hemispherical analyser having resolution of 1.0 eV. The binding energies obtained in the XPS analysis were calibrated against the C1s peak at 284.6 eV.

IO@NiNPs catalyzed hydrogenation reaction was monitored on PerkinElmer Lambda 35 UV–vis spectrophotometer by corresponding $\lambda_{max}$. Hydrogenation reaction monitoring was also done by thin-layer chromatography (TLC, Using ninhydrin as staining reagent) and gas chromatography (GC). All products of the reduction of nitroarenes are commercially available and were identified by comparing their physical and spectral data (m.p., TLC (silica gel 60 F254, Merck, Mumbai, India), GC (Perkin Elmer clarus 500 GC) and $^{1}$H NMR (BRUKER 400 MHz) with those of authentic samples or reported data.

## Acknowledgement

The authors are grateful to the Solvay group, new Research, Development and Technology Centre at savli, Gujarat, India, for financial assistance.

## Captions to the Figures

**Scheme-1** Schematic representation of IO@NiNPs catalysed reduction of PNA to PPDA by $NaBH_4$.

**Scheme-2** General scheme for reduction of various Nitro aromatics.

**Fig. 1** XRD pattern of (A) Iron oxide and (B) IO@NiNPs.

**Fig.2** (A) EDX patterns and (B) Magnetic hysteresis curve of as-prepared IO and IO@NiNPs.

**Fig.3** X-ray photoelectron spectra of IO@NiNPs

**Fig.4** HR-TEM images of magnetic IO@NiNPs at different magnifications (A) 20nm;(B) 10nm and (C) 5nm showing particle size distribution; The resolved lattice fringes and SAED pattern of IO@NiNPs are (D), (E) and (F) respectively.

**Fig.5** UV-vis spectra indicating the conversion of *p*-Nitroaniline to *p*-Phenylenediamine in presence of IO@NiNPs.

**Fig.6** (A) Reaction mixture of PPDA (a) before and (b) after magnetic separation by simple magnet; HR-TEM of reused magnetic IO@NiNPs at different magnifications (B) 20 nm, (C) 0.2 μm, (E) 1nm (lattice fringes) and (F) SAED pattern of IO@NiNPs

## References


1. (a) P. T. Anastas and J. C. Warner, *Green Chemistry Theory and Practice*, Oxford University Press, Oxford, 1998; (b) A. S. Matlack, *Introduction to Green Chemistry*, Marcel Dekker, New York, 2001;(c) J. H. Clark and D. J. Macquarrie, *Handbook of Green Chemistry and Technology*, Blackwell Publishing, Abingdon, 2002; (d) V. Polshettiwar and R. S. Varma, *Chem. Soc. Rev.*, 2008, **37**, 1546.
2. (a) V. Polshettiwar and R. S. Varma, *Aqueous Microwave Chemistry*, RSC Publishing, Cambridge, 2010; (b) V. Polshettiwar and R. S. Varma, *Acc. Chem. Res.*, 2008, **41**, 629; (c) R. B. N. Baig and R. S. Varma, *Chem. Commun.*, 2012, **48**, 5853; (d) R. B. N. Baig and R. S. Varma, *Chem. Soc. Rev.*, 2012, **41**, 1559.
3. (a) S. Wittmann, A. Shatz, R. N. Grass, W. J. Stark and O. Reiser, *Angew. Chem., Int. Ed.*, 2010, **49**, 1867; (b) M. Benaglia, Recoverable and Recyclable Catalysts, John Wiley & Sons, Chichester, 2009.(c) V. Polshettiwar and R. S. Varma, *Green Chem.*, 2010, **12**, 743.
4. (a) F. Alonso, P. Riente and M. Yus, *Acc. Chem. Res.*, 2011, **44**, 379; (b) F. Alonso and M. Yus, *Pure Appl. Chem.*, 2008, **80**, 1005; (c) N. Yan, C. Xiao and Y. Kou, *Coord. Chem. Rev.*, 2010, **254**, 1179; (d) S. Shylesh, V. Schnemann and W. R. Thiel, *Angew. Chem. Int. Ed.*, 2010, **49**, 3428; (e) V. Polshettiwar, R. Luque, A. Fihri, H. Zhu, M. Bouhrara and J-M. Basset, *Chem. Rev.*, 2011, **111**, 3036.
5. (a) R. B. N. Baig and R. S. Varma, *Chem. Commun.*, 2013, **49**, 752; (b) V. Polshettiwar and R. S. Varma, *Green Chem.*, 2010, **12**, 743–754
6. (a) T. Hirakawa and P. V. Kamat, *J. Am. Chem. Soc.*, 2005, **127**, 3928; (b) Y. J. Huang, X. C. Zhou, M. Yin, C. P. Liu and W. Xing, *Chem. Mater.*, 2010, **22**, 5122;

(c) J. X. Wang, H. Inada, L. J. Wu, Y.M. Zhu, Y.M. Choi, P. Liu,W. P. Zhou and R. R. Adzic, *J. Am. Chem. Soc.*, 2009, 131, 17298; (d) K. Bakhmutsky, N. L. Wieder, M. Cargnello, B.Galloway, P. Fornasiero and R. J. Gorte, *Chem Sus Chem*, 2012, **5**, 140; (e) H. L. Jiang, T. Akita and Q. Xu, *Chem. Commun.*, 2011, **47**, 10999; (f) J. Bao, J. He, Y. Zhang, Y. Yoneyama and N. Tsubaki, *Angew. Chem., Int. Ed.*, 2008, **47**, 353; (g) H. L. Jiang, T. Akita, T. Ishida, M. Haruta and Q. Xu, *J. Am. Chem. Soc.*, 2011, **133**, 1304; (q) R. G. Chaudhuri and S. Paria, *Chem. Rev.*, 2012, **112**, 2373 and references cited therein.

7. M. B. Gawande, H. Guo, A. K. Rathi, P. S. Branco, Y. Chen, R. S. Varma and D-L. Peng, *RSC Adv.*, 2013, **3**, 1050 and references cited therein.
8. V. Polshettiwar, R. Luque, A. Fihri, H. Zhu, M. Bouhrara, and J-M. Basset, *Chem. Rev.*, 2011, **111**, 3036.
9. P. S. Haddad, T. M. Martins, L. D. Souza-Li, L. M. Li, K. Metze, R. L. Adam, M. Knobel and D. Zanchet, *Mater. Sci. Eng.*, 2008, **28**, 489‑494.
10. S. Si, A. Kotal, T. K. Mandal, S. Giri, H. Nakamura and T. Kohara, *Chem. Mater.*, 2004, **16,** 3489.
11. A. Zablotskaya, I. Segal, E. Lukevics, M. Maiorov, D. Zablotsky, E. Blums, I. Shestakova and I. Domracheva, *J. Magn. Magn. Mater.*, 2009, **321**, 1428.
12. W. Cai and J. Wan, *J. Colloid Interface Sci.*, 2007, **30**, 366.
13. D. Maity and D. C. Agrawal, *J. Magn. Magn. Mater.*, 2007, **308**, 46.
14. S. K. Das, S. Kumar and P. Ramachandrarao, *Waste Manag.*, 2000, **20**, 725.
15. H. Yu, X. Xue and D. Huang, *Mater. Res. Bull.*, 2009, **44**, 2112.
16. C. Li, H. Sun, Z. Yi and L. Li, *J. Hazard. Mater.*, 2010, **174**, 78.

17. L. Zeng, X. Li and J. Liu, *Water Res.*, 2004, **38**, 1318.

18. S. Zhang, S. Xue, X. Liu, P. Duan, H. Yang, T. Jiang, D. Wang and R. Liu, *J. Min. Sci.*, 2006, **42**, 403.

19. S. K. Giri, N. N. Das, G. C. Pradhana, *Coll Surf A*, 2011, **389**, 43.

20. (a) A. M. Tafesh and J. Weiguny, *Chem. Rev.*, 1996, **96**, 2035; (b) Jr. R. J. Rahaim and Jr. R. E. Maleczka, *Org. Lett.*, 2005, **7**, 5087; (c) S. Chandrasekhar, S. J. Prakash and C. L. Rao, *J. Org. Chem.*, 2006, **71**, 2196; (d) Q. Shi, R. Lu, L. Lu, X. Fu and D. Zhao, *Adv. Synth. Catal.*, 2007, **349**, 1877.

21. (a) C. Yu, B. Liu and L. Hu, J. Org. Chem., 2001, 66, 919–924, and references therein; (b) A. K. Shil and P. Das, *Green Chem.*, 2013, DOI: 10.1039/C3GC41179F

22. A. Saha and B. Ranu, *J Org Chem*, 2008, **73**, 6867 and references therein

23. A. Corma and P. Serna, *Science*, 2006, **313**, 332.

24. (a) N. Sahiner, S. Butun and P. Ilgin, *Coll Surf A*, 2011, **386**,16; (b) M. B. Gawande, A. K. Rathi, P. S. Branco, I. D. Nogueira, A. Velhinho, J. J. Shrikhande, U. U. Indulkar, R. V. Jayaram, C. A. A. Ghumman, N. Bundaleski, and O. M. N. D. Teodoro, *Chem. Eur. J.*, 2012, **18**, 12628; (c) R. Dey, N. Mukherjee, S. Ahammed and B. C. Ranu, *Chem. Commun.*, 2012, **48**, 7982.

25. (a) P. S Rathore, J. Advani, S. Rathore and S. Thakore, *J Mol Catal A: Chem*, 2013, **377**, 129; (b) P. S Rathore, R. Patidar, S. Rathore and S. Thakore, *Catal Lett*, 2013, DOI 10.1007/s10562-013-1168-2

26. W. Kim, C-Y. Suh, S-W. Cho, K-M. Roh , H. Kwon, K. Song and I-J. Shon, *Talanta*, 2012, **94**, 348.

27. Y. Ren, R. Cingolani, R. Buonsanti, P. D. Cozzoli, V. Petkov, *J. Am. Chem. Soc.*, 2009, **131**, 14264.

28. N. Kimizuka, S. Sasaki and K. Tsukimura, *Jpn. J. Appl. Phys., Part 1*, 1997, **36**, 3609.

29. A. P. Grosvenor, M. C. Biesinger, R. St. C. Smart and N. S. McIntrye, *Surf. Sci.*, 2006, **600**, 1771.

30. D. Maiti, U. Manju, S. Velaga and P. S. Devi, *Cryst. Growth Des.*, 2013, **13**, 3637

31. (a) X. Huang, X. Liao and B. Shi, *Green Chem*, 2011, **13**, 2801; (b) P. Herve´s, M. Pe´ rez-Lorenzo, L. M. Liz-Marza´n, J. Dzubiella, Y. Lu and M. Ballauff, *Chem. Soc. Rev.*, 2012, **41**, 5577.

32. Z. Jiang, J. Xie, D. Jiang, X. Wei and M. Chen, *Cryst Eng Comm*, 2013, **15**, 560–569.

33. Y. Kojima and T. Haga, *Int J Hydrogen En*, 2003, **28**, 989.

34. (a) J. J. Spivey, G. W. Roberts, B. H. Davies, Catalyst Deactivation, Elsevier, Amsterdam, 2001; (b) F. Alonso, P. Riente, J. A. Sirvent, M. Yus, *Appl. Catal. A: Gen.*, 2010, **378**, 42.

35. (a) M. Valodkar, P. S. Rathore, R. N. Jadeja, M. Thounaojam, R. V. Devkar and S. Thakore, *J. Hazar. Mater.*, 2012, **201-202**, 244;(b) J. M. Yan, X. B. Zhang, S. Han, H. Shioyama and Q. Xu, *Inorg. Chem.*, 2009, **48**, 7389.

36. V. S. Madeira, 2010. Coal Mine Residues Recycling for the Fabrication of High Added Value Products. Ph.D. thesis. Federal University of Santa Catarina, Brazil (in Portuguese).

37. S. L. F. Andersen, R. G. Flores, V. S. Madeira, H. J. José and R. F. P. M. Moreira, *Ind. Eng. Chem. Res.*, 2012, **51**,767.

38. R. G. Flores, S. L. F. Andersen, L. K. K. Maia, H. J. José and R. F. P. M. Moreira, *J. Environ. Manage*., 2012, **111**, 53.

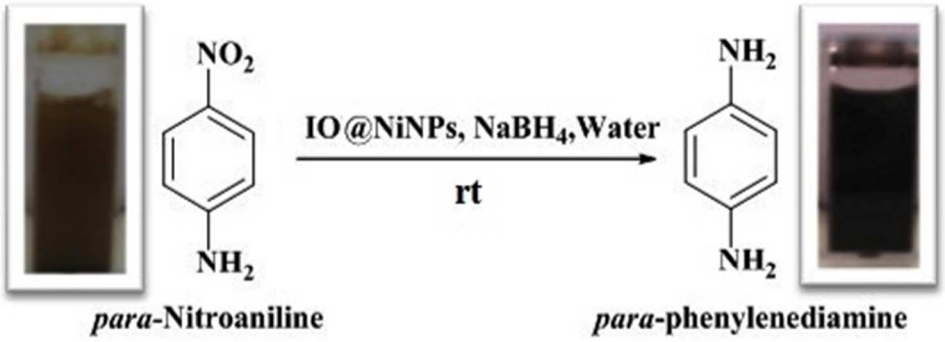


**Scheme-1**

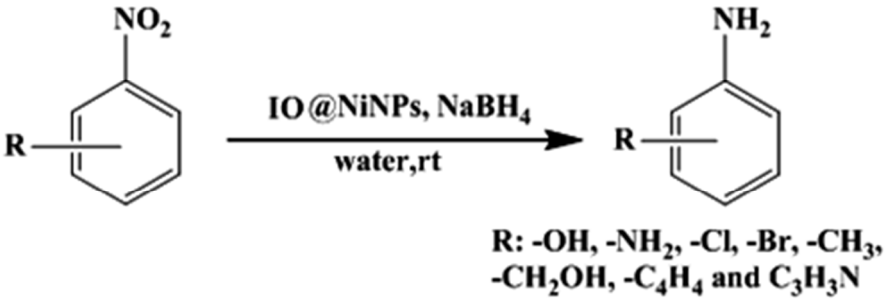


**Scheme-2**

**Table-1 Optimization of reaction conditions for hydrogenation of *p*-Nitroaniline.**

| Sr. No. | Catalyst (mg) (IO@NiNPs) | $NaBH_4$ (mmol) | Temperature (°C) | Time (h\min) | %Yield[b] |
|---|---|---|---|---|---|
| 1 | none | None | 25-30 to reflux | 24h | - |
| 2 | 12 | ,, | ,, | ,, | < 5 |
| 3 | none | 1.85 | ,, | ,, | < 10 |
| 4 | IO[c] | 1.85 | rt | ,, | 55 |
| 5 | 12 | 1.85 | ,, | 12min | 96 |
| **6[a]** | **12** | **1.44** | **,,** | **12min** | **96** |
| 7 | ,, | 1.03 | ,, | 20min | ,, |
| 8 | ,, | 0.61 | ,, | 30min | ,, |
| 9 | ,, | 0.20 | ,, | 24h | 90 |
| 10 | ,, | 0.02 | ,, | 24h | 40 |
| 11 | 18 | 1.44 | ,, | 12 | 96 |
| 12 | 15 | ,, | ,, | 12 | ,, |
| 13 | 9 | ,, | ,, | 23 | ,, |
| 14 | 6 | ,, | ,, | 32 | ,, |
| 15 | 3 | ,, | ,, | 39 | ,, |
| 16 | 0.3 | ,, | ,, | 180 | ,, |

Reaction conditions: *p*-Nitroaniline-0.362 mmol, solvent 2 mL (water), a-optimized reaction condition, b- Isolated yield, and c-Iron oxide only (20mg).

**Table-2 Chemoselective Reduction of Nitroaromatics to Aromatic Amines at rt by IO@NiNPs.**

| S. No | Substrate | Product | Time (min±2) | Yield[a] (%±3) | TON(±2)/TOF ($min^{-1}$)[b] |
|---|---|---|---|---|---|
| 1 | *o*-Nitrotoluene | *o*-Toulidine | 24 | 89 | 106/4.45 |
| 2 | *p*-Nitrotoluene | *p*-Toulidine | 13 | 92 | 110/8.49 |
| 3 | *m*-Nitrotoluene | *m*-Toulidine | 16 | 94 | 112/7.05 |
| 4 | *o*-Nitrophenol | *o*-Aminophenol | 09 | 92 | 110/12.26 |
| 5 | *p*-Nitrophenol | *p*-Aminophenol | 10 | 90 | 108/10.8 |
| 6 | *m*-Nitrophenol | *m*-Aminophenol | 17 | 90 | 108/6.3 |
| 7 | *p*-Nitrobenzyl alcohol | *p*-Aminobenzyl alcohol | 13 | 89 | 106/8.15 |
| 8 | *m*-Nitrobenzyl alcohol | *m*-Aminobenzyl alcohol | 13 | 94 | 112/8.61 |
| 9 | *o*-Nitrobenzyl alcohol | *o*-Aminobenzyl alcohol | 15 | 95 | 114/7.6 |
| 10 | 4-Chloro-3-nitro aniline | 4-Chlorobenzene-1,3-diamine | 30 | 91 | 109.2/3.64 |
| 11 | 4-Chloro-2-nitro aniline | 4-Chlorobenzene-1,2-diamine | 40 | 90 | 108/2.7 |
| 12 | Nitrobenzene | Aniline | 25 | 95 | 114/4.56 |
| 13 | *o*-Nitroaniline | *o*-Phenylenediamine | 16 | 94 | 112.8/7.05 |
| 14 | *m*-Nitroaniline | *m*-Phenylenediamine | 14 | 94 | 112.8/8.05 |
| 15 | *p*-Nitroaniline | *p*-Phenylenediamine | 12 | 96 | 115/9.6 |
| 16 | *o*-Chloronitobenzene | *p*-Chloroaniline | 19 | 93 | 111.6/5.87 |
| 17 | *m*-Chloronitobenzene | *m*-Chloroaniline | 22 | 94 | 112.8/5.12 |
| 18 | *p*- Bromonitobenzene | *p*- Bromoaniline | 17 | 95 | 114/6.7 |
| 19 | *o*-Bromonitobenzene | *o*-Bromoaniline | 21 | 95 | 114/5.4 |
| 20 | *m*-Bromonitobenzene | *m*-Bromoaniline | 29 | 94 | 112/3.86 |

| | | | | | |
|---|---|---|---|---|---|
| 21 | 6-Nitroquinoline | Quinolin-6-amine | 35 | 94 | 112/3.2 |
| 22 | 1-Nitronaphthalene | 1-Naphthylamine | 38 | 93 | 111.6/2.93 |
| 23 | 4-chloro-2-methyl-1-nitrobenzene | 2-Amino-5-Chlorotoluene | 50 | 88 | 105.6/2.11 |
| 24 | 3-Nitroquinoline | Quinolin-3-amine | 40 | 92 | 110.4/2.76 |
| 25 | 1,3-dinitrobenzene | *m*-Phenylenediamine | 30 | 89 | 106.8/3.56 |
| 26 | 1,2-dinitrobenzene | *o*-Phenylenediamine | 28 | 85 | 102/3.64 |
| 27 | 1,4-dinitrobenzene | *p*-Phenylenediamine | 28 | 92 | 110.4/3.94 |

Reaction conditions: All reactions were carried at rt, substrate-0.362 mmol, catalyst-12mg (0.45wt% or 1.06 mol% NiNPs of Substrate), $NaBH_4$-1.44 mmol and solvent 2mL (water), (a) Isolated yield after column chromatography (b) TON and TOF was calculated on basis of NiNPs

**Table-3 Reduction of PNA to PPDA at rt (25-30°C using IO@NiNPs in optimum condition (Recycling experiments)**

| Cycle | Time(min±2) | Yield[a](±1%) | IY[b](±3%) | Cycle | Time(min) | Yield[a](±1%) | IY[b](±3%) |
|---|---|---|---|---|---|---|---|
| 1 | 12 | 98 | 96 | 16 | 22 | 99 | 96 |
| 2 | 12 | 99 | 96 | 17 | 30 | 98 | 96 |
| 3 | 14 | 98 | 96 | 18 | 36 | 98 | 96 |
| 4 | 13 | 98 | 96 | 19 | 35 | 99 | 95 |
| 5 | 13 | 98 | 96 | 20 | 42 | 99 | 95 |
| 6 | 16 | 98 | 96 | 21 | 45 | 99 | 96 |
| 7 | 15 | 97 | 96 | 22 | 46 | 99 | 96 |
| 8 | 16 | 98 | 96 | 23 | 45 | 99 | 96 |
| 9 | 21 | 98 | 96 | 24 | 45 | 98 | 95 |
| 10 | 25 | 98 | 96 | 25 | 47 | 99 | 96 |
| 11 | 24 | 99 | 96 | 26 | 45 | 98 | 96 |
| 12 | 21 | 99 | 96 | 27 | 44 | 99 | 96 |
| 13 | 25 | 98 | 96 | 28 | 59 | 98 | 96 |
| 14 | 21 | 98 | 96 | 29 | 70 | 98 | 95 |
| 15 | 24 | 98 | 96 | 30 | 140 | 98 | 96 |

(a) GC yield, (b) Isolated yield

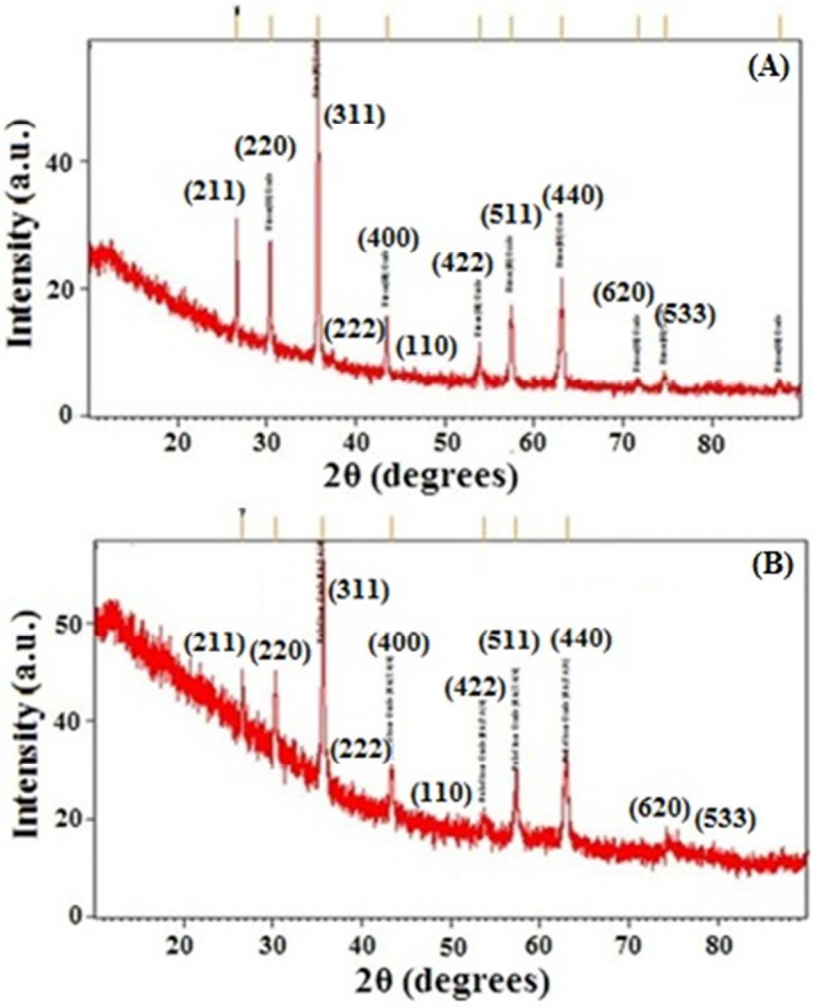


**Fig. 1**

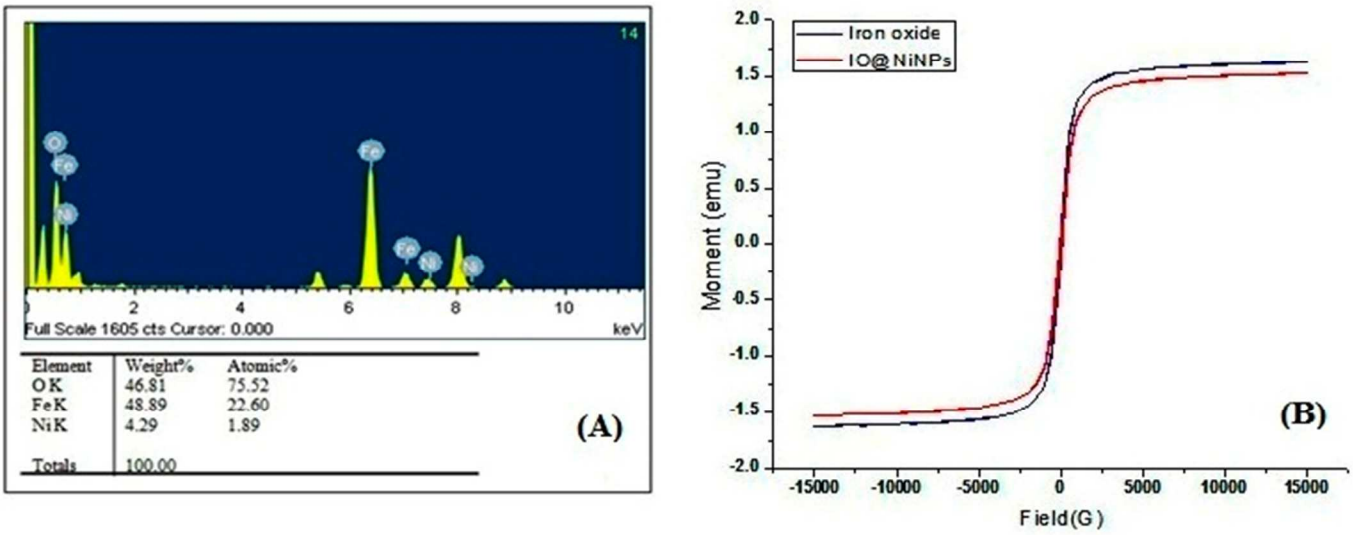


**Fig. 2**

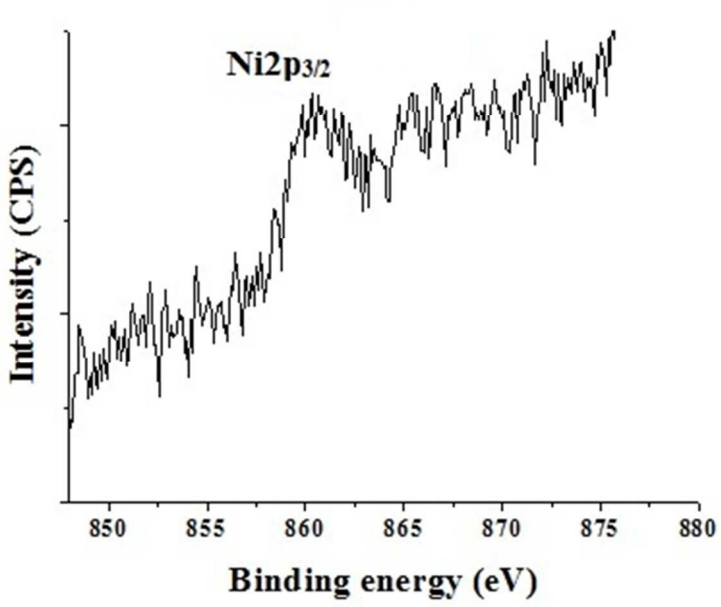


**Fig. 3**

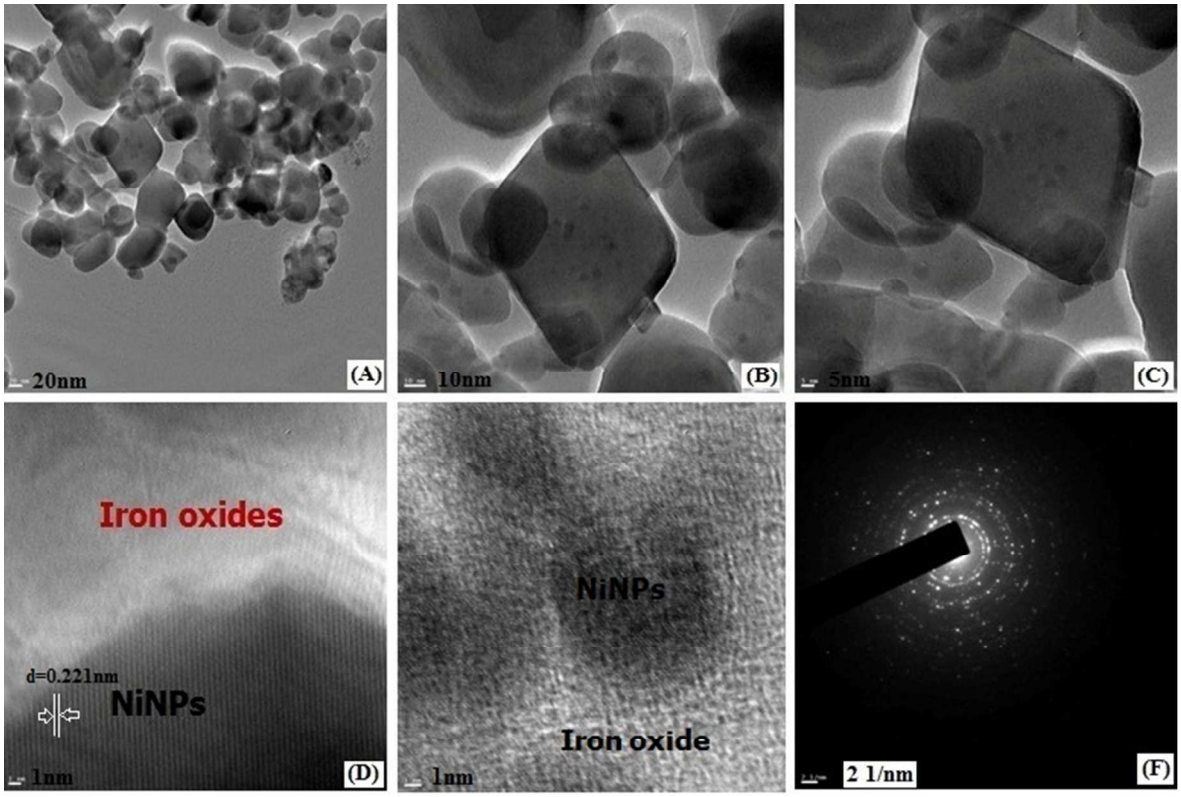


**Fig. 4**

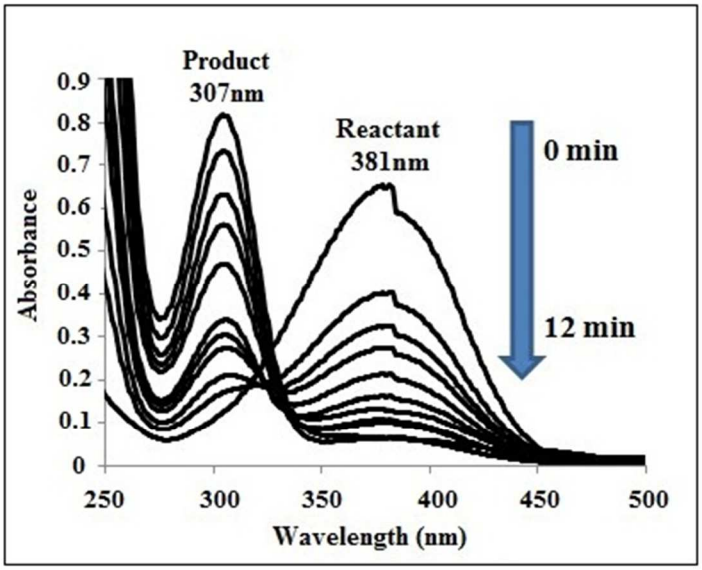


**Fig. 5**

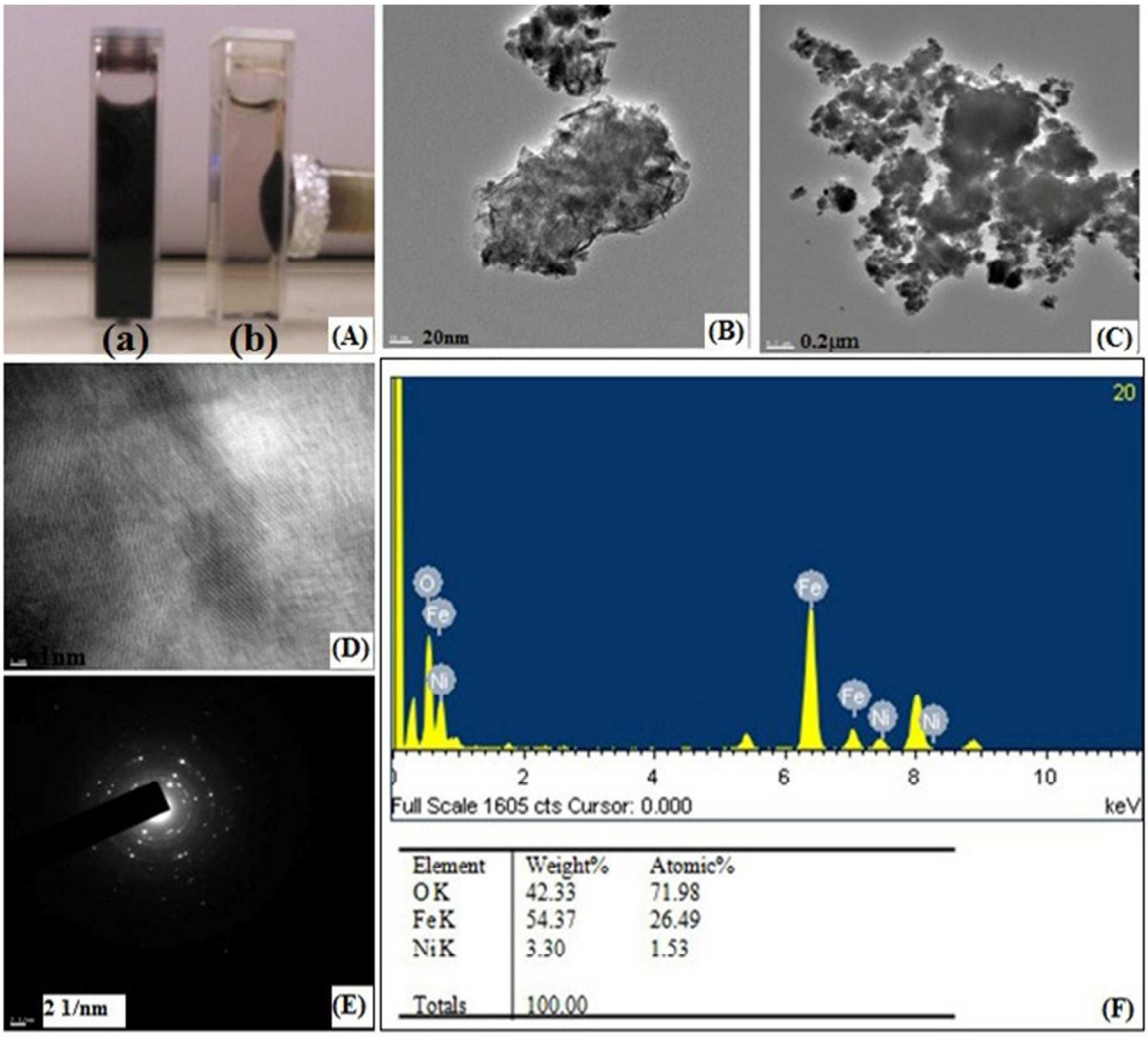


**Fig. 6**